Advances in feedback control of the Rijke tube thermoacoustic instability

Simon J. Illingworth[a,*], Aimee S. Morgans[b]
[a]*Department of Engineering, University of Cambridge, UK*
[b]*Department of Aeronautics, Imperial College London, South Kensington, London, UK*

Abstract

This paper considers methods for the feedback control of thermoacoustic oscillations. Two distinct approaches to the problem are considered. The first is robust model-based control, which involves two stages: finding a model of the system, and designing a controller based on that model. The focus is on using model reduction techniques to find a low-order, balanced model of the Rijke tube which, despite having few degrees of freedom, is useful for feedback control design purposes. The second approach uses adaptive (or self-tuning) control, which does not require a model of the system, but instead requires that it meets some general properties. The focus here is on reducing how much must be known *a priori* about the plant. Specifically, an adaptive controller is considered which does not require knowledge of the sign of the plant's high-frequency gain, and this is done by employing a Nussbaum gain. The controllers are successfully applied in experiments on a Rijke tube. Both controllers completely eliminate oscillations, and in both cases stability is maintained following a large change in operating conditions.

Keywords: combustion oscillations, thermoacoustics, feedback flow control, adaptive flow control, reduced-order modeling

1. INTRODUCTION

Thermoacoustic instability can occur in any system where combustion takes place within an acoustic resonator, and is caused by a coupling between unsteady heat release and acoustic waves. Unsteady combustion is an efficient acoustic source [1], and combustors tend to be highly resonant systems, which together can lead to self-excited oscillations by the following mechanism, first described by Rayleigh [2]. Pressure waves, generated by unsteady heat release at the flame, reflect from the combustor boundaries and arrive back at the flame. If the phase relationship is suitable, their interaction with the flame gives rise to further unsteady heat release, which in turn generates more pressure waves, completing the natural feedback loop. See Candel [3] for a review of combustion oscillations.

Many of the earliest studies of thermoacoustic instability were for liquid-propellant rocket motors in the 1950s and 1960s [4], research that was motivated by the stability problems encountered in those devices. More recently, the problem of thermoacoustic stability has been encountered in low NO_x gas turbine applications, where using lean premixed combustion makes the combustor especially prone to oscillations [5, 6], and this has motivated a great deal of research on the subject [7, 8].

Many different strategies for eliminating thermoacoustic instability have been considered, and these can be split into two broad categories: passive control, which relies on some modification of the system's geometry or boundary conditions to affect the system; and active control, which uses actuation to provide external energy. Active control can be further divided into open-loop and closed-loop control schemes. In open-loop active control, no sensors are used and the forcing is 'blind' – the actuation does not depend on the measurement of any parameter of interest. McManus et al. [9] review open-loop (and early closed-loop) control studies of combustion oscillations.

Closed-loop (or 'feedback') control, like open-loop control, uses an actuator (typically a loudspeaker or fuel injector) to provide external energy to the system. The crucial difference is that the

* Corresponding author.
Email address si250@cam.ac.uk (S. J. Illingworth).

Preprint submitted to International Journal of Flow Control *February 26, 2011*

actuation is in response to a measured signal (most commonly pressure). Closed-loop control therefore has three essential ingredients: sensors for the measurement of some system parameter; actuators to alter the system in some way; and a feedback law by which the actuators respond to the sensor measurements. Such closed-loop strategies are the focus of the more recent review by Dowling and Morgans [10], and the focus of this paper.

The first experimental closed-loop control studies were performed on the Rijke tube [11], and shortly afterwards on an afterburner [12] and on a turbulent ducted flame [13]. Those early studies all involved simple phase-shift or time-delay control loops. Gulati and Mani [14] showed the inadequacies of such controllers, and demonstrated the improved closed-loop performance of a controller designed using the frequency response of the system and Nyquist techniques. Since then, model-based control techniques have been promoted [15, 16] and many such studies have been performed. In any model-based control scheme, there are two pertinent issues to address. First, a model of the system must be available. This can come from a physics-based model [17, 18] or, less commonly, directly from experiments using system identification techniques – which could involve finding a mathematical model [19] or measuring the frequency response directly [16]. (The dynamical processes involved in large- and full-scale systems, such as combustion and turbulence, are too complex for physics-based models to be useful, and so system identification techniques are crucial for model-based control at these scales.) Second, a framework for the controller design must be chosen, and this has typically involved Linear Quadratic control or some variant [20, 19], Nyquist techniques [14, 16] or $\mathcal{H}_\infty$ loop-shaping [21, 17].

Another type of control scheme which has received attention is adaptive control, where the controller adapts to changes in the system, thereby maintaining control over a wide range of operating conditions. The first 'dynamic' adaptive controllers for combustion oscillations (using concomitant sensing and actuation timescales) were Least Mean Squares (LMS) controllers [22]. Since then neural networks [23] and observer-based adaptive controllers [24] have also been considered. More recently, a class of self-tuning regulators has been considered [25]. The adaptive tuning of the control parameters is based on finding a Lyapunov function which reduces in amplitude with time when the control parameters are updated in the right way. Annaswamy et al. [26] looked at such an adaptation scheme for a specific combustion system, and Evesque et al. [27] followed by considering a scheme that was valid for a whole class of combustion systems. Determining an accurate model of a combustion system which is useful for feedback control purposes is one of the most difficult aspects of model-based feedback control, and so the advantages of adaptive control are clear. No such model is required, and instead only minimal information about the system is needed. This is particularly true of the self-tuning regulators of [26] and [27], since only some very general assumptions about the combustion system are made.

This paper investigates model-based and adaptive control of thermoacoustic oscillations, using the Rijke tube as its experimental test bed. The paper is organized as follows. In §2 the Rijke tube is introduced and its open-loop transfer function is derived using a simple analytical model. The experimental arrangement is also introduced, and a method for finding the *linear* transfer function from experimental data is described. In §3, model-based feedback control is considered. The focus is on finding a simple, low-order model of the Rijke tube which is useful for feedback control design. In §4, adaptive (or self-tuning) feedback controllers are considered. Such controllers require little information about the system, and the focus here is on reducing this further by considering an adaptive controller which does not require knowledge of the high-frequency gain (defined in due course) of the open-loop system.

2. THE RIJKE TUBE

The Rijke tube provides a simple means of generating combustion oscillations on a laboratory scale. It consists of a vertical cylindrical tube open at both ends, with a heat source inside the tube some distance from the lower end. Large-amplitude acoustic oscillations are excited when the heat source is in the lower half of the tube [28].

2.1. Open-loop transfer function

In this section we use some simple physics to find an analytical expression for the open-loop transfer function between a pressure forcing signal (provided by a loudspeaker) and a pressure measurement downstream of the flame. We will not use this analytical expression directly for controller design, nor will we compare it to the open-loop transfer function that we will find using the Eigensystem

Realization Algorithm in §3. (For a comparison of the analytical model developed here with that found experimentally using system identification techniques, see Dowling and Morgans [10].) The reason we include the analysis here is to show how the Rijke tube's transfer function is affected by its geometry, boundary conditions, flame dynamics and sensor location.

The analysis used here is the same as that used by Dowling and Morgans [10]. Consider the Rijke tube arrangement shown in figure 1. In analyzing the system we assume that the frequencies of interest are sufficiently low that the combustion zone is short compared to the acoustic wavelengths; that there is negligible mean flow; that entropy waves can be neglected; and that the mean density $\overline{\rho}$ and speed of sound $\overline{c}$ remain constant throughout the tube. (Changes in $\overline{\rho}$ and $\overline{c}$ have little effect on the system's stability characteristics [29].)

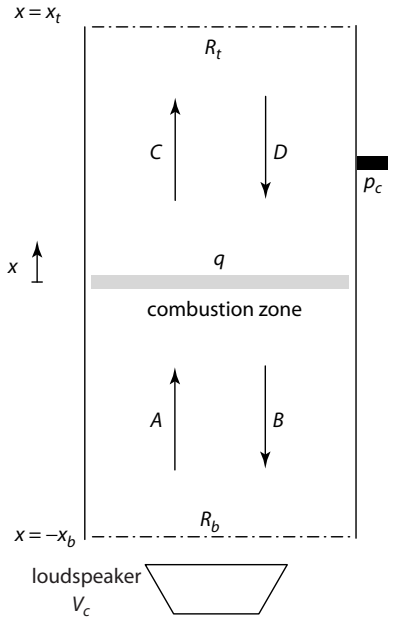

Figure 1: Schematic of the Rijke tube model used to form an analytical expression for the open-loop transfer function.

Downstream of the combustion zone (region 2, which is where the pressure sensor lies), the pressure obeys the linear wave equation and so the pressure and velocity can be written as

$$p_2(x,t) = C\left(t - \frac{x}{c}\right) + D\left(t + \frac{x}{c}\right) \tag{1}$$

$$u_2(x,t) = \frac{1}{\overline{\rho}\overline{c}}\left[C\left(t - \frac{x}{c}\right) - D\left(t + \frac{x}{c}\right)\right]. \tag{2}$$

(Similarly, the pressure and velocity upstream of the flame (region 1) can be written in terms of the waves $A(t)$ and $B(t)$.)

The inward-traveling waves $A(t)$ and $D(t)$ can be related to the outward-traveling waves $B(t)$ and $C(t)$ by introducing reflection coefficients at the bottom and top boundaries. For the upstream wave $A(t)$, there will also be a contribution from the loudspeaker pressure signal, which we label $L(t)$.

To relate the acoustic waves either side of the combustion zone, the linearized conservation equations can be used [30]. For negligible mean flow these require zero pressure difference and a velocity jump that is related to the heat release rate. We model the rate of unsteady heat release per unit area q by relating it to the unsteady velocity just upstream of the flame, which in the Laplace domain can be written as

$$q(s) = \overline{\rho c}^2 H(s) u_1(s) . \tag{3}$$

Here $H(s)$ is the flame transfer function.

By combining the acoustic equations; the boundary conditions; the conditions across the flame zone; and the unsteady combustion model, and then taking Laplace transforms, we can relate the outward traveling waves $B(s)$ and $C(s)$ to the loudspeaker pressure signal $L(s)$:

$$\begin{bmatrix} -1 - R_b e^{-s\tau_b} & 1 + R_t e^{-s\tau_t} \\ \left[1 - R_b e^{-s\tau_b}\right] F(s) & 1 - R_t e^{-s\tau_t} \end{bmatrix} \begin{bmatrix} B(s) \\ C(s) \end{bmatrix} = \begin{bmatrix} e^{-sx_b/c} \\ F(s) e^{-sx_b/c} \end{bmatrix} L(s), \tag{4}$$

where $F(s) = [1 + (\gamma - 1)H(s)]$, $\tau_b = 2x_b/c$ and $\tau_t = 2x_t/c$.

We are interested in a pressure measurement downstream of the combustion zone, so we first solve eqn (4) for $C(s)$. Then using eqn (1) for the acoustics we can solve for the pressure at some downstream location x_c. Introducing a loudspeaker transfer function $W_c(s)$, which relates the control voltage $V_c(s)$ to the pressure signal $L(s)$, $W_c(s) = L(s)/V_c(s)$, we finally arrive at

$$P(s) = \frac{p_c(s)}{V_c(s)} = \frac{-2W_c(s)e^{-s(x_c + x_b)/c}}{J(s)}[1 + R_t e^{-2s(x_t - x_c)/c}]F(s), \tag{5}$$

where $J(s)$ is the determinant of the 2×2 matrix in eqn (4).

Therefore the poles (or eigenvalues) of the open-loop system are determined by the 2×2 matrix in eqn (4), and we see that they depend on the reflection coefficients at the boundaries R_b and R_t, the acoustic propagation times τ_b and τ_t, and the flame transfer function $H(s)$.

2.2. Location of the system zeros

As well as considering the system poles, it is also important to consider its zeros (i.e. those values of s where $P(s) = 0$) because these are also important for feedback control. In particular, any zeros in the right half of the complex s-plane will make feedback control more difficult [31, chap. 5]. Furthermore, the adaptive controller that we will develop in §4 requires that any zeros are in the left half-plane. From eqn (5) we see that there are three sources of zeros: the loudspeaker transfer function $W_c(s)$, the reflection coefficients term $[1 + R_t e^{-2s(x_t - x_c)/c}]$, and the term $F(s) = [1 + (\gamma - 1)H(s)]$, which is related to the flame dynamics. We now treat each of these terms in turn.

The zeros contributed by $W_c(s)$ will of course depend on the loudspeaker dynamics. We make the assumption here that the loudspeaker does not introduce any right half-plane zeros, which is a reasonable assumption for a simple loudspeaker.

A necessary (but not sufficient) condition for $[1 + R_t e^{-2s(x_t - x_c)/c}] = 0$ is that $e^{-2Re(s)(x_t - x_c)/c} = 1/|R_t|$. Therefore if R_t satisfies $|R_t| < 1$ then any zeros arising from this term are guaranteed to be in the left half-plane. That $|R_t| < 1$ is a reasonable assumption to make for the low Mach-number flow in the Rijke tube, which allows us to assume that this term will introduce left half-plane zeros only. (At a higher (non-negligible) Mach number M, the theoretical reflection coefficient at an open boundary becomes $-(1 + M)/(1 - M)$, which means it may in this case exceed 1, even in the presence of damping [32].)

Finally, the zeros contributed by the term $F(s) = [1 + (\gamma - 1)H(s)]$ will depend on the flame dynamics H(s). Physically, these zeros are the result of a cancellation of two sources of acoustic waves: those caused by unsteady heat release; and those generated directly by the loudspeaker. (Notice that, unlike the zeros of the term $[1 + R_t e^{-2s(x_t - x_c)/c}]$, these zeros are independent of the sensor location x_c.) The flame dynamics are in general too complex to make any general statements on this term, but we make three observations here. The first is that if we adopt a simple model of the flame which includes a gain and a time delay, $H(s) = ke^{-s\tau}$, then we see that a necessary (but again, not sufficient) condition for the zeros is that

$$e^{-\mathrm{Re}(s)\tau} = \frac{1}{|k|}\frac{1}{\gamma - 1}, \tag{6}$$

from which we see that right half-plane zeros can occur if $|k| > 1/(\gamma - 1)$. The second observation is that despite this possibility for right half-plane zeros (which still exists for more complex flame dynamics), no right half-plane zeros are present in the open-loop transfer function to be presented in §3. The third observation, and the one that is most encouraging, is that this source of zeros is linked to the loudspeaker actuation, and is not a general feature of feedback-controlled combustion systems. If we instead used a valve to modulate the fuel flow rate to the combustion zone – which is the most

practical means of actuation at large- and full-scale – then this source of zeros would disappear. See Morgans and Annaswamy [32], where the open-loop transfer function is derived for this type of actuation, and where no such zeros occur.

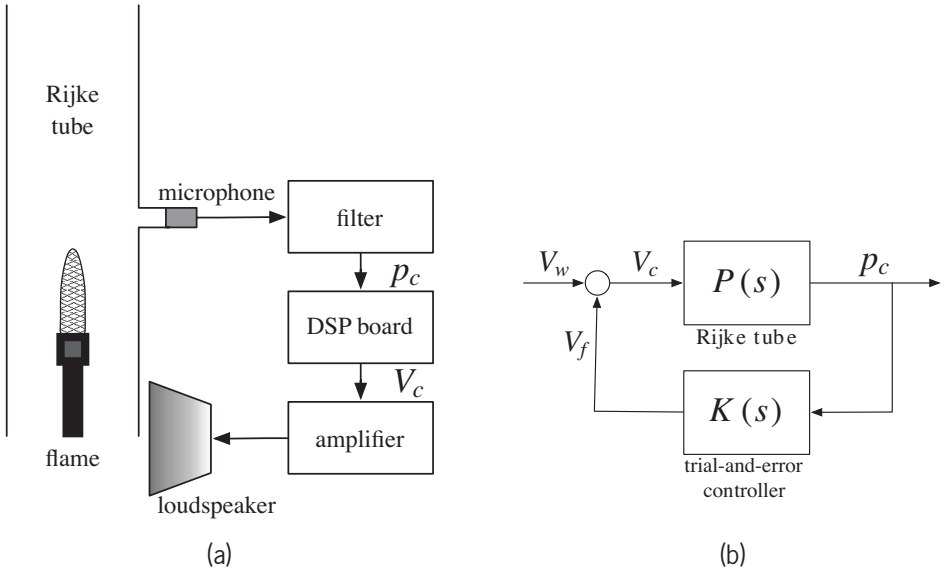

Figure 2: Experimental set-up of the Rijke tube: (a) schematic; and (b) corresponding block diagram for the system linearization.

2.3. Experimental arrangement

The Rijke tube used is the same as that used by Morgans and Dowling [16]. It consists of a cylindrical quartz tube of length 750 mm and diameter 44 mm inclined vertically as shown in figure 2(a). A propane-fuelled Bunsen burner provides a laminar flame which is stabilized on a grid 210 mm above the bottom of the tube. In these experiments a variable length trombone-like attachment is also used, which allows the length of the Rijke tube to be varied between 750 mm and 1030 mm. The Rijke tube exhibits instability over the entire range of this variable length, the frequency of the instability varying from 246 Hz at a length of 750 mm, to 193 Hz at a length of 1030 mm. (In §3.1 a linear model will be found for the Rijke tube at a length of 890 mm, which exhibits oscillations at a frequency of 227 Hz in the absence of control.)

Measurement of the pressure perturbation (denoted p_c) is provided by a condenser microphone fitted to a tube tapping situated 410 mm from the bottom of the tube. The semi-infinite line technique is used to obtain thermal insulation without distortion from acoustic reflections. Actuation is achieved using a 50 W low-frequency loudspeaker (with the control voltage to the loudspeaker before amplification denoted V_c – see figure 2(a)) situated close to the lower end of the tube. The loudspeaker exhibits a flat frequency response over the frequency range of interest (50–2000 Hz). Outside of this range, its dynamics become more complicated. To eliminate these dynamics, a bandpass filter is applied to the microphone signal with a pass-band from 50 Hz to 2000 Hz.

The controllers to be presented are implemented on a TI C6713DSK DSP board with ADC and DAC evaluation modules (an ADS8361EVM and a DAC7731EVM). The pressure measurement p_c and control voltage V_c are recorded using a PC-based data acquisition system. The sampling frequency for both the DSP board and the data acquisition system is 5000 Hz.

2.4. Finding the Rijke tube's linear dynamics

In §3, linear model-based control techniques will be used to design robust feedback controllers for the Rijke tube, and clearly such techniques require a linear model of the Rijke tube. This is challenging, because the growing amplitudes of the unstable thermoacoustic oscillations will ultimately give rise to non-linear limit-cycling behaviour.

One solution to this problem is to acquire the model at a stable operating point which is close to the unstable case of interest. This stable system will have a linear response to (sufficiently small) forcing,

and one hopes that a controller designed for this stable system will also be successful for the unstable system of interest. This approach was successfully used for combustion oscillations by Langhorne et al. [33] and by Tierno and Doyle [21].

A second solution, and the solution used in this paper, is to first stabilize the system using feedback, and to measure the response to forcing of the (linear) system operating in closed-loop. This approach has been used successfully for combustion oscillations before by Morgans and Dowling [16], and is shown schematically in figure 2(b), where P(s) is the open-loop system of interest and $K(s)$ is a feedback controller. The controller used to stabilize (and therefore linearize) the Rijke tube is a manually-tuned, trial-and-error phase-shift controller.

The total input voltage V_c in figure 2(b) is given by $V_c = V_w - V_f$ (negative feedback convention), where V_w is a forcing signal and V_f is the control voltage from the feedback controller. The system's *open-loop* transfer function P(s) is then given by

$$P(s) = \frac{p_c(s)}{V_c(s)}.$$

Therefore despite the system's operating in closed-loop, its open-loop dynamics are recovered. (If instead the forcing signal V_w were used as the system input, the *closed-loop,* stabilized transfer function would be found.)

One must ensure that the system is responding linearly to the forcing signal u_w for the forcing amplitudes used. This was verified for both systems by checking that the controlled system satisfied both the additive property $y(u_1 + u_2) = y(u_1) + y(u_2)$ and the homogeneous property $y(\alpha u) = \alpha y(u)$.

One may now ask: if the Rijke tube is already stabilized, why do we need to design a controller for it? The answer lies in the superior performance of a model-based controller: the initial stabilizing controller is found by trial-and-error, but feedback control is most successful when an accurate model of the system-to-be-controlled is available. In §3 we will see that by using an accurate model of the Rijke tube, control can be achieved over a wide range of operating conditions.

A disadvantage of the present method is that the dynamics generating the instability need to reasonably simple (in some sense) for the Rijke tube to be stabilized by trial-and-error in the first place. There are two things that one should keep in mind concerning this point. First, a model-based controller should provide stability over a range of open-loop plants, and this means that one can start with a relatively 'gentle' instability, and then apply the controller so-designed at a more challenging design point. One may even design the controller for a nearby stable operating point, and reasonably expect that the controller will be successful on the unstable plant: this has previously been achieved [33, 21]. Second, it has been acknowledged for some time that there are advantages to performing system identification in *closed-loop* rather than in open-loop [34], since it is the closed-loop behaviour that one is ultimately interested in. Indeed, given two systems (which could represent two different operating conditions, for example), it is possible for those systems to be very similar in their open-loop behaviour, yet very different in closed-loop (and vice versa) [35], which further motivates this approach.

3. ROBUST FEEDBACK CONTROL USING A REDUCED-ORDER MODEL

This section looks at the first of the two approaches for feedback control: synthesizing a regulator using model-based control techniques. There are two steps to such an approach: first find a model of the system, and then design a regulator based on that model, and these two steps constitute two important decisions for any model-based control approach. The first of these is addressed in §3.1, where the method for finding a model of the Rijke tube is described, and the second is addressed in §3.2, where the choice of regulator, the Linear Quadratic Gaussian (LQG) regulator, is introduced.

3.1. Reduced-order modeling using the ERA

Finding simple dynamical models of the Rijke tube is crucial if model-based control techniques are to be successful. 'Simple' here means two things in particular: that the model is linear; and that the model is low-order (equivalently, that it has a small number of degrees of freedom). The first of these requirements has already been addressed in §2.4. The second requirement is the focus of this section. There are a number of options for forming low-order models of fluid systems (which are governed by partial differential equations and are therefore infinite-dimensional). Perhaps the most commonly used is the Proper Orthogonal Decomposition (POD), also known as principal component analysis, or the Karhunen-Loeve expansion. The resulting POD modes are optimal in that they maximize the average

energy in the projection of the data onto the subspace spanned by the modes. However, these POD modes may not be the best modes for describing the *dynamics* that generate the data set, and these dynamics are crucial when one is interested in a model for feedback control purposes.

Recent work by Rowley [36] and by Ma et al. [37] has demonstrated the importance of using reduced-order models that are *balanced,* at least when those models are to be used for feedback control design. The balancing refers to the observability and controllability Gramians of the resulting reduced-order model being equal and diagonal. As their names suggest, these Gramians are linked to the observability and controllability of the model, and these two concepts are important for reduced-order modeling. Referring to eqn (7), observability is concerned with the *measurement* of the state x, while controllability is concerned with the *manipulation* of that state. Physically, the Gramians being equal and diagonal means that the dynamics that generate the data set are properly taken into account. These notions are discussed in more detail in Appendix A, where the observability and controllability Gramians are also defined.

To form a reduced-order model of the Rijke tube, the Eigensystem Realization Algorithm (ERA) is used [38, 39], which gives a balanced, reduced-order state-space model of the system (in discrete-time) of the form:

$$\begin{aligned} x(k+1) &= Ax(k) + Bu(k) \\ y(k) &= Cx(k)\ . \end{aligned} \tag{7}$$

Here $u \in \mathbb{R}^p$ is the system input, $y \in \mathbb{R}^q$ is the system output, $x \in \mathbb{R}^n$ is the system state, and A, B, C are suitably-dimensioned matrices.[1] The ERA is explained in more detail in Appendix A. The ERA has been used for fluids before. Cattafesta et al. [40] and Cabell et al. [41] used it for flow control purposes, but as a system identification technique rather than for model reduction. Gaitonde and Jones [42] used it to form a reduced-order model of a CFD scheme, and Silva and Bartels [43] used it for reduced-order modeling of aeroelastic flutter, but neither of these studies was concerned with feedback control of the flow. For more details on the ERA specifically for fluid flows, see [37, 44, 45, 46].

The state-space model used is eighth-order ($n = 8$), which was found to be adequate to capture the most dominant dynamics of the Rijke tube. This is shown clearly in figure 3, where the frequency response (or transfer function) of the eight-state, balanced model is compared in a Bode diagram to that found using spectral analysis [47] (which rather than giving a reduced-order model, gives the complex-valued response at a discrete set of frequencies). The phase increase seen across the first mode at 227 Hz indicates that the corresponding eigenvalues (or poles) are in the right half of the complex plane, and therefore unstable. The phase decrease across the second mode at 680 Hz indicates that the corresponding poles are in the left half-plane, and therefore stable. Note that the zeros seen at frequencies of approximately 445 Hz and 1320 Hz can both be attributed to the reflection coefficients term $[1 + R_t e^{-2s(x_t - x_c)/c}]$ in eqn (5) which, provided $R_t < 1$, will always be in the left half-plane for any arrangement of the Rijke tube.

One observes that the eight-state model captures these first two modes of the Rijke tube, and we will see in §3.3 that this is sufficient for feedback control design.

3.2. LQG regulator design

We now look at the subject of Linear Quadratic Gaussian (LQG) regulator design, which will use the reduced-order model to form a feedback controller for the Rijke tube. A closed-loop control arrangement for some general plant $P(s)$ is shown in figure 4. Here $K(s)$ is the closed-loop regulator-to-be-designed. The effect of noise (n) and disturbances (d) is included. For the discrete-time state space model defined by eqn (7), a Linear Quadratic (LQ) regulator uses the state feedback law

$$u = -\Gamma x \tag{8}$$

to minimize the quadratic cost function

$$J = \sum_{i=0}^{\infty} \left(x^T Q_x x + u^T Q_u u \right). \tag{9}$$

[1] Because the system is unstable, an extension to the ERA called Observer/Controller Identification (OCID) [39] is used.

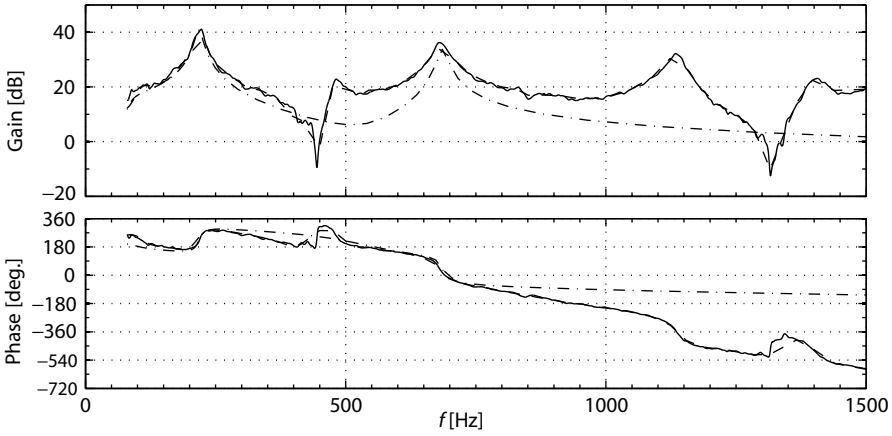

Figure 3: The open-loop transfer function found using spectral analysis (———) is compared to that found using the eight-state balanced model (-·-·-·-).

$Q_x \in \mathbb{R}^{n \times n}$ and $Q_u \in \mathbb{R}^{p \times p}$ are weighting matrices used to penalize large system states and large control inputs respectively. The Rijke tube has a single input ($u = V_c$), and so Q_u in eqn (9) is simply a scalar. The output measurement ($y = p_c = Cx$) is chosen as the output cost (giving $Q_x = C^T C$), and the quadratic cost function has the simple form:

$$J = \sum_{i=0}^{\infty} \left(p_c^2 + q_u V_c^2 \right),$$

where the scalar q_u is used to specify the relative importance of maintaining a small input signal (V_c) and maintaining a small output measurement (p_c). The value used is $q_u = 7.10$.

Substituting eqn (8) into eqn (7), we obtain the closed-loop system

$$\begin{aligned} x(k+1) &= (A - B\Gamma)x(k) \\ y(k) &= Cx(k) \end{aligned} \tag{10}$$

and we see that, by suitable choice of the feedback gain matrix Γ, the eigenvalues of $(A - B\Gamma)$ – and therefore the dynamics of the closed-loop system – can be made stable.

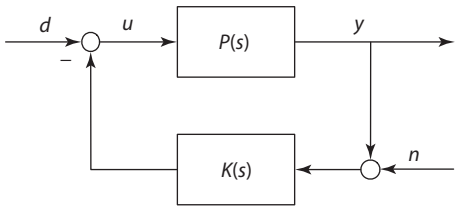

Figure 4: General closed-loop control arrangement. The effect of noise (n) and disturbances (d) is included.

Linear Quadratic (LQ) control assumes that the full state x is available to the regulator - this state is used in the feedback law (8). In many cases, though, the full state is not available for measurement, the regulator having direct access only to the inputs u and the outputs y. *Linear Quadratic Gaussian* (LQG) control remedies this by using an observer to form an estimate $\hat{x}$ of the real state x. This estimate of the state is used in the LQG control feedback law

$$u = -\Gamma \hat{x}.$$

It remains to see how the estimate of the state $\hat{x}$ is formed. The *Gaussian* term in Linear Quadratic Gaussian control refers to the specific type of observer used, a Kalman filter. A Kalman filter amounts to a specific choice of the observer which is optimal, in the sense that the error converges in the presence of stochastic disturbances d and noise n (see figure 4), assumed to be zero-mean, *Gaussian,* white-noise processes. The covariances used in the Kalman filter design are $E(dd^T) = 3.0 \times 10^{-4}$ and $E(nn^T) = 2.1 \times 10^{1}$.

The LQG and optimal estimation problems can be solved using standard routines in Matlab. The resulting LQG controller and observer can then be combined to give an overall regulator $K(s)$, which is of the same order as the plant model used $P(s)$.

It should be noted that although the LQ control problem has guaranteed stability margins, there are no such guaranteed margins for the LQG control problem [48], and therefore the stability margins must be checked for a given control design. In practice, though, LQG control often gives very satisfactory results, and this will be seen in the next section.

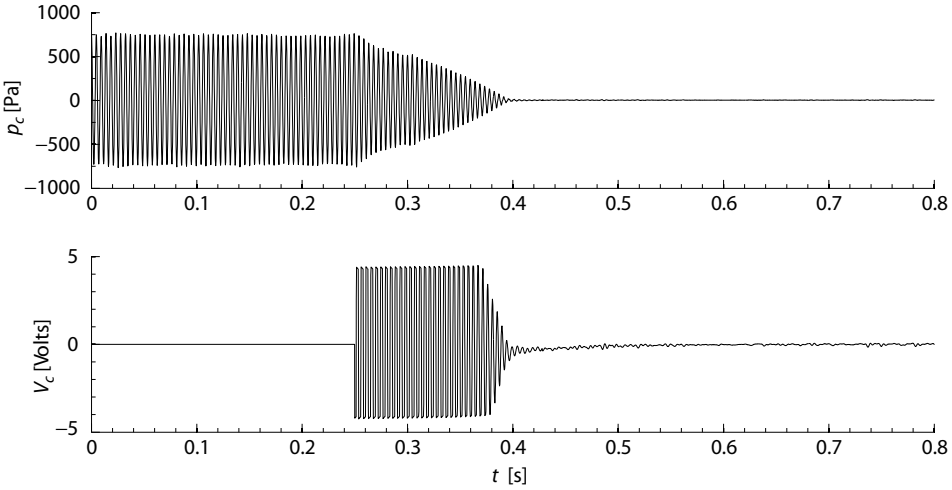

Figure 5: Closed-loop control of the Rijke tube at the design length of 890 mm.

3.3. Experimental results

We now look at applying the LQG regulator to the Rijke tube experiment. The LQG regulator is first applied at the design length of 890 mm. The robustness of the regulator is then tested by applying it at an off-design length of 750 mm.

Closed-loop control results for the design length of 890 mm are shown in figure 5. Control is activated after 0.25s, by which time the Rijke tube is exhibiting limit-cycle oscillations. The LQG regulator stabilizes the Rijke tube, and the pressure measurement is reduced to the background noise level within approximately 0.15s.

Figure 6 shows the results of the LQG regulator applied at the off-design length of 750 mm. The regulator still provides closed-loop stability when control is activated after 0.25s, and the pressure measurement is still reduced to the background noise level, demonstrating the robustness of the controller. The off-design Rijke tube length represents a change of –15.7% from the nominal length. Comparing this

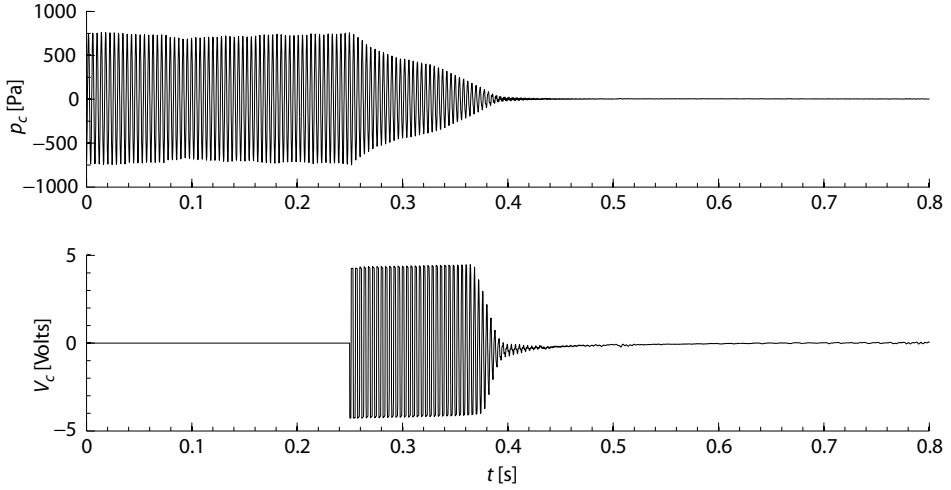

Figure 6: Closed-loop control of the Rijke tube at the off-design length of 750 mm.

with the original trial-and-error controller makes clear the advantages of the model-based control approach: this original controller loses stability following a change in length of less than 3.0 %.

A few remarks are in order here, first concerning the order of the Rijke tube's state-space model, and second concerning the Rijke tube's linearity.

The eight-state reduced-order model captures the first two modes of the Rijke tube, but in many ways it is most important to capture the first (unstable) mode, and to do this a reduced-order model with just two states suffices. Closed-loop control experiments were also performed using an LQG regulator based on this two-state model, and closed-loop stability was still achieved, even as the Rijke tube's length was varied. However, one must also consider that, although the higher-order modes do not need to be stabilized by the controller, they could be *destabilized* by it, and so in practice, accounting for them with a higher-order model is wise.

The state-space model found represents the *linear* dynamics of the Rijke tube, but the controller is activated from within a pressure limit-cycle, which is certainly not linear. Such behaviour – where linear control methods stabilize the non-linear system – has been seen previously in closed-loop control studies of combustion oscillations, and Dowling [30] provides an explanation for it using describing function analysis. We will see the same kind of behaviour for the adaptive controller, considered next.

Finally, we have seen that the LQG regulator is sufficiently robust to deal with the dynamical differences brought about by the change in length, but we have not attempted to quantify this. This could be achieved using the ν-gap metric [35], which is the most useful measure of distance between systems when one is concerned specifically with applying feedback to those systems. The ν-gap metric fits very naturally into an $\mathcal{H}_\infty$ loop-shaping control design, and this would be an interesting area for future work.

4. ADAPTIVE CONTROL FOR UNKNOWN CONTROL DIRECTION

This section represents a significant break from the previous section, where model-based feedback control methods were used. Here the focus is instead on adaptive (or self-tuning) control, which requires no model, but instead requires that the system meet certain general properties. The work presented here is intended as an extension of previous work on adaptive control of combustion oscillations [27, 49, 50].

Throughout this section, the adaptive controllers considered amount to a simple proportional gain controller, i.e. $u(t) = -k(t)y(t)$, the adaptation made clear in this equation by the feedback gain $k(t)$ being a function of time. The adaptive control problem is then concerned with providing an updating rule for $k(t)$.

First in this section, the high-frequency gain of a system is defined, and its importance for Lyapunov-based adaptive control is discussed. A Lyapunov-based adaptive controller is then introduced, which provides an updating rule for $k(t)$, but which requires knowledge of the sign of the system's high-frequency gain to do it. This leads to the main contribution of this section: an adaptive controller which, by employing a *Nussbaum gain,* does not require knowledge of the high-frequency gain of the system. The controller is first introduced, and then applied successfully to the Rijke tube, where it eliminates thermoacoustic oscillations.

4.1. Importance of the high-frequency gain

Lyapunov-based adaptive control – so-called because of its foundations in Lyapunov stability theory – is a well-established method for the adaptive stabilization of unknown systems, and relies on finding a suitable Lyapunov function, via which closed-loop stability can be proved. A Lyapunov function is always positive-definite and can therefore be thought of as an energy function. The time derivative of the Lyapunov function is guaranteed to be negative if the time derivative of a control vector is updated in the right way. Therefore when the right updating rule is used, the Lyapunov function is guaranteed to decrease monotonically in time, and the control vector is guaranteed to converge to a stabilizing set.

At the heart of Lyapunov-based adaptive control are three assumptions [51]. If the open-loop system has transfer function $P(s)$, and if we write $P(s)$ as the ratio of two co-prime, monic polynomials

$$P(s) = g_o \frac{N_P(s)}{D_P(s)},$$

then the three conditions placed on $P(s)$ are [51]:

(i) The sign of the high-frequency gain g_o is known.
(ii) The relative degree n^* of $P(s)$ is known.[2] (I)
(iii) The zeros of $P(s)$ are all stable (i.e. $P(s)$ is minimum phase).

It is the first condition that we concern ourselves with here. For many systems, the sign of the high-frequency gain (whose physical significance is given in the following) is obvious from the physics of the problem, and so providing it poses no problem.

Combustion systems, however, are infinite-dimensional, and so the sign of the high-frequency gain is unknown. There are two ways to view this infinite-dimensionality. The first is to consider that the system is governed by partial, rather than ordinary, differential equations, which have an infinite number of degrees of freedom. The second is by looking at eqn (5), where we see that the open-loop transfer function involves time delay terms of the form $e^{-s\tau}$. This time delay term is not rational: it cannot be written as the ratio of two polynomials in s.[3] The phase of a pure time delay evaluated at frequency $s = i\omega$, that is $e^{-i\omega\tau}$, is $-\omega\tau$, which evolves indefinitely with frequency. Therefore the sign of the high-frequency gain of a pure time delay is not defined.

Physical significance of the high-frequency gain

To demonstrate the physical significance of the high-frequency gain, we now look at a simple first-order unstable system whose transfer function is

$$P(s) = \frac{y(s)}{u(s)} = \frac{g_o}{s - a}, \tag{11}$$

where u is the system input, y is the system output, s is the Laplace variable like before, g_o is the high-frequency gain of the system and a (which is positive for an unstable system) corresponds to the location of the system's (only) pole. In the time domain, this corresponds to the first-order differential equation

$$\dot{y}(t) = ay(t) + g_o u(t) \ .$$

Looking at $\dot{y}(t)$ for small time using the initial value theorem, and for a unit step input $u(s) = 1/s$:

$$\lim_{t\to 0} \dot{y}(t) = \lim_{s\to\infty} s^2 y(s)$$

$$= \lim_{s\to\infty} s^2 \frac{1}{s} \frac{g_o}{s - a}$$

$$= g_o .$$

Therefore knowing the *sign* of the high-frequency gain corresponds to knowing, in the time domain, the sign of the system's 'instantaneous gain': that is, knowing whether the system's response to a positive unit step input is positive or negative for t sufficiently small. More generally, for an n^{th} order system with a relative degree of n^*, the same analysis can be applied to the $(n^*)^{\text{th}}$ derivative of the output, $y^{(n^*)}$.

Importance for feedback control

The term 'high-frequency gain' is perhaps a little misleading in some respects: it suggests that $\text{sgn}(g_0)$ is only important because of its influence at high frequencies. Yet the results of §3, where the reduced-order model is not at all accurate at high frequencies (see in particular figure 3), suggests that what happens at high frequencies is not important for feedback control. Why then is sgn (g_0) important? We will now see, via a simple example, that sgn (g_0) is important for feedback control because it dictates the system's 'control direction' (which explains the title of this section).

[2] The relative degree is defined as $n^* = \deg[D_P(s)] - \deg[N_P(s)]$, which can be thought of as the system's 'pole excess', i.e. the number of poles minus the number of zeros.

[3] Although it could be approximated by a rational function by using a Pade approximant, for example.

Consider a plant $P(s)$ given by the first-order system (11), this time acted upon by a feedback controller $K(s)$. (Such an arrangement was shown in figure 4.) Consider the special case when the feedback controller is simply a (fixed, for the moment) proportional gain, $K(s) = k$, so that $u = -ky$. Then the closed-loop transfer function $P_{cl}(s)$ is given by

$$P_{cl}(s) = \frac{P(s)}{1 + kP(s)} = \frac{g_0}{s + (kg_0 - a)}.$$

Since the proportional gain k acts to stabilize the system by moving the closed-loop system's pole into the left half plane (i.e. by making the term $(kg_o - a)$ positive), we see that the proportional gain k must be both of the correct sign (so that the product kg_o is positive) and sufficiently large so that $kg_o > a$. Therefore the sign of g_0 dictates the sign of k required for closed-loop stability. Again, this result holds for any n^{th} order system, as long as it has a *relative* degree n^* of one. (It can be shown, using root locus arguments, that any minimum phase system with a relative degree of one can be stabilized using a proportional feedback gain alone.)

Importance for Lyapunov-based adaptive control

We now look at how these arguments apply to Lyapunov-based adaptive control. A system of relative degree one that satisfies the three conditions (I) can be stabilized using a proportional feedback gain [52]. We have seen that this feedback gain needs to be (i) of sufficient magnitude and (ii) of the right sign. For a Lyapunov-based adaptive controller, the second condition must be provided via knowledge of the sign of the high-frequency gain, which is used to form an adaptive controller with updating rule and control law

$$\dot{k}(t) = \text{sgn}(g_o)y^2(t) \tag{12a}$$

$$u(t) = -k(t)y(t). \tag{12b}$$

It is clear how $\text{sgn}(g_o)$ is used in (12a) to decide in which direction to update the control gain $k(t)$ (since $y^2(t) \geq 0$). The adaptive controller is then guaranteed to meet the first condition and provide closed-loop stability, the proof of closed-loop stability being asserted using a suitable Lyapunov function.

4.2. Adaptive control using a Nussbaum gain

Morse [53] suggested that knowledge of the sign of the high-frequency gain was intrinsic: in particular, that a linear plant *cannot* be stabilized without knowledge of $\text{sgn}(g_o)$. Nussbaum [54] proved this conjecture for first order *rational* controllers. More importantly, however, by using a non-rational term he constructed a globally adaptively stabilizing controller for a first order system which did not rely on knowledge of the sign of g_o. The work of Willems and Byrnes [55] extends Nussbaum's result to any minimum-phase system with a relative degree of one.

The controllers used in those two studies both incorporate a *Nussbaum gain* $N(k)$. Willems and Byrnes [55] show that for the control of a minimum phase system with a relative degree of one, any function $N(k)$ which satisfies the conditions

$$\begin{aligned} \sup_{k>0} \frac{1}{k}\int_0^k N(\sigma)d\sigma &= \infty \\ \inf_{k>0} \frac{1}{k}\int_0^k N(\sigma)d\sigma &= -\infty \end{aligned} \tag{13}$$

is a Nussbaum gain and guarantees closed-loop stability for unknown $\text{sgn}(g_0)$. Such a Nussbaum gain can be used with the updating rule and control law

$$\begin{aligned} \dot{k}(t) &= y^2(t) \\ u(t) &= -N(k)y(t) \end{aligned}$$

to adaptively stabilize the system. These equations are very similar to the updating rule (12a) and control law (12b) used for the Lyapunov controller. The key difference is that the Nussbaum gain – and the conditions placed upon it – remove the need for knowledge of $\text{sgn}(g_o)$.

Functions satisfying (13) are a type of switching function. The review paper of Ilchmann [56] gives some examples of such functions, including:

$$N_1(k) = k^2 \cos k$$
$$N_2(k) = k \cos \sqrt{|k|}.$$

It is now clear how the Nussbaum gain achieves control without knowledge of the sign of the high-frequency gain. The conditions imposed upon a Nussbaum gain (13) mean that it sweeps across both positive and negative gains, while also increasing in magnitude with increasing k: in contrast to the Lyapunov-based adaptive controller, a Nussbaum gain automatically meets *both* requirements for closed-loop stability. For a proof of the closed-loop stability provided by a Nussbaum gain, see Appendix B.

In closed-loop control, unnecessarily high feedback gains are to be avoided, not least because they can place high demands on the actuator, and because they can lead to excitation of other modes of the system. Using a Nussbaum gain which is a smooth function helps to alleviate any high gain behaviour of the Nussbaum gain. Furthermore, one can help to ensure that the final stabilizing Nussbaum gain, N^*, is in the vicinity of the minimum required, and not significantly larger, by observing that the Nussbaum gain only need switch sign once, if at all. This is explained more fully in Appendix C, where choosing the adaptation rate μ (introduced presently in eqn (14c)) is discussed.

4.3. Experimental results

Two sets of experimental results are now presented.[4] First, for fixed operating conditions, the Nussbaum controller achieves control even when it is first updated in the wrong direction. Second, the robustness of the controller is investigated by changing the length of the Rijke tube after control at the nominal length has been achieved. Control is maintained following this change. To the authors' knowledge, it represents the first experimental results for a Nussbaum-type adaptive controller.

The specific updating rule and control law used are

$$\dot{k}(t) = \gamma\, p_c^2(t) \tag{14a}$$
$$V_c(t) = -N(k) p_c(t), \tag{14b}$$

and the Nussbaum gain is

$$N(k) = k \cos(\mu |k|^{\frac{1}{4}}), \tag{14c}$$

with $\gamma = 1.24 \times 10^{-7}$ and $\mu = 2.93$. Here γ and μ are the adaptation rates of the controller, explained in more detail in Appendix C.

The theoretical development of the Nussbaum gain ignores the influence of noise in the system. Since noise will always be present in the pressure measurement p_c (even when the system has been stabilized), we see from eqn (14a) that $k(t)$ will never be stationary. This problem can be solved by introducing a *dead-zone* into the updating rule [57]. With this modification, $k(t)$ is only updated if the pressure p_c exceeds some pre-defined limit (which is chosen based on the magnitude of the noise in the system). The updating rule for k(t) then becomes

$$\dot{k}(t) = \begin{cases} \gamma\, p_c^2(t) & |p_c(t)| \geq P_{d.z.} \\ 0 & |p_c(t)| < P_{d.z.} \end{cases}, \tag{15}$$

with $P_{\text{d.z.}} = 37$ Pa in this particular case, which is about 5 % of the limit-cycle amplitude.

Figure 7(a) shows adaptive control results when the Nussbaum gain is initially updated in the right direction. The pressure perturbation has already established a limit cycle when control is activated at $t = 0.2$s. Since the Nussbaum gain is initially updated in the right direction, the cosine term in the Nussbaum gain (14c) does not switch sign. Hence in this case the controller behaves much like a

[4] The experimental results reported in this section and in §3 were performed at different times (approximately 2 years apart). In this time the Rijke tube did not change, but the amplifier used did. Referring to figure 2, the amplifier is included in the model of the plant, $P(s)$, and therefore the results reported here are effectively for a different open-loop system to that presented in §3.

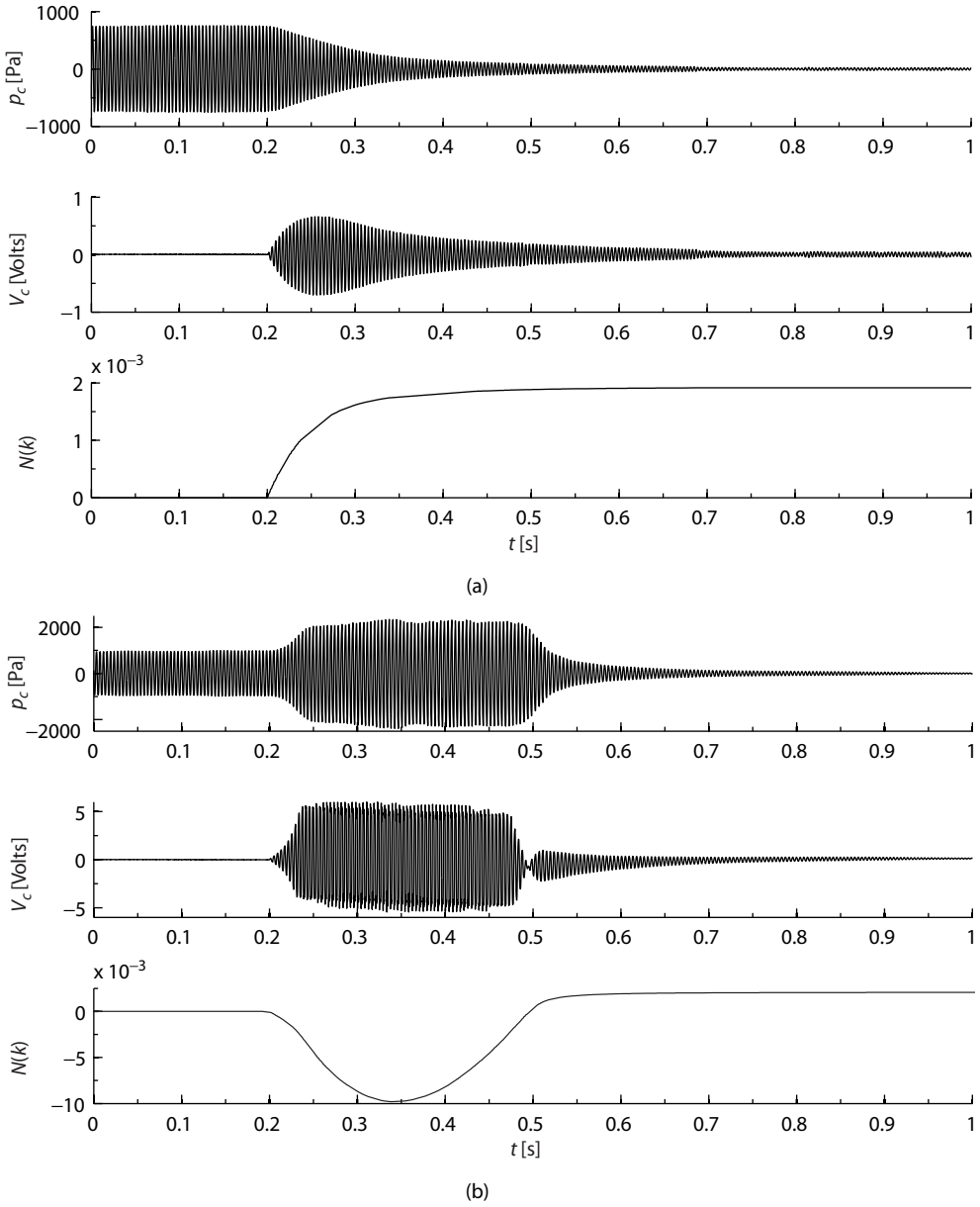

Figure 7: Experimental results for fixed operating conditions: with (a) $N(k)$ initially updated in the right direction; and (b) $N(k)$ initially updated in the wrong direction. In both cases the measured pressure perturbation p_c, control voltage V_c and Nussbaum gain $N(k)$ are shown.

Lyapunov-based adaptive controller, and the tuning of the Nussbaum gain $N(k)$ is very similar to that of the adaptive parameter k.[5] Within approximately 0.5s of control being activated, the controller finds a stabilizing gain N^*, and oscillations are eliminated.

Figure 7(b) shows adaptive control results when the Nussbaum gain is initially updated in the wrong direction. The impact of this is clear: when control is first activated at $t = 0.2$s, the Nussbaum gain $N(k)$ causes the Rijke tube's limit cycle to actually increase in amplitude. Soon after, however, the Nussbaum gain changes sign and finds a stabilizing gain N^* which is both of sufficient magnitude and of the right sign. The system is stabilized within approximately 0.4s of control being activated. The value of the Nussbaum gain used in this case is 2.26×10^{-3}, compared with 1.91×10^{-3} in figure 7(a).

The robustness of the adaptive controller is now considered by increasing the length of the Rijke tube after control at the nominal length has been achieved – the length of the tube is increased from 750 mm to 870 mm. Results are shown in figure 8(a), where control is activated at $t = 0.2$s, again from

[5] k starts from zero here (i.e. $k(0) = 0$), which is true for all three experiments.

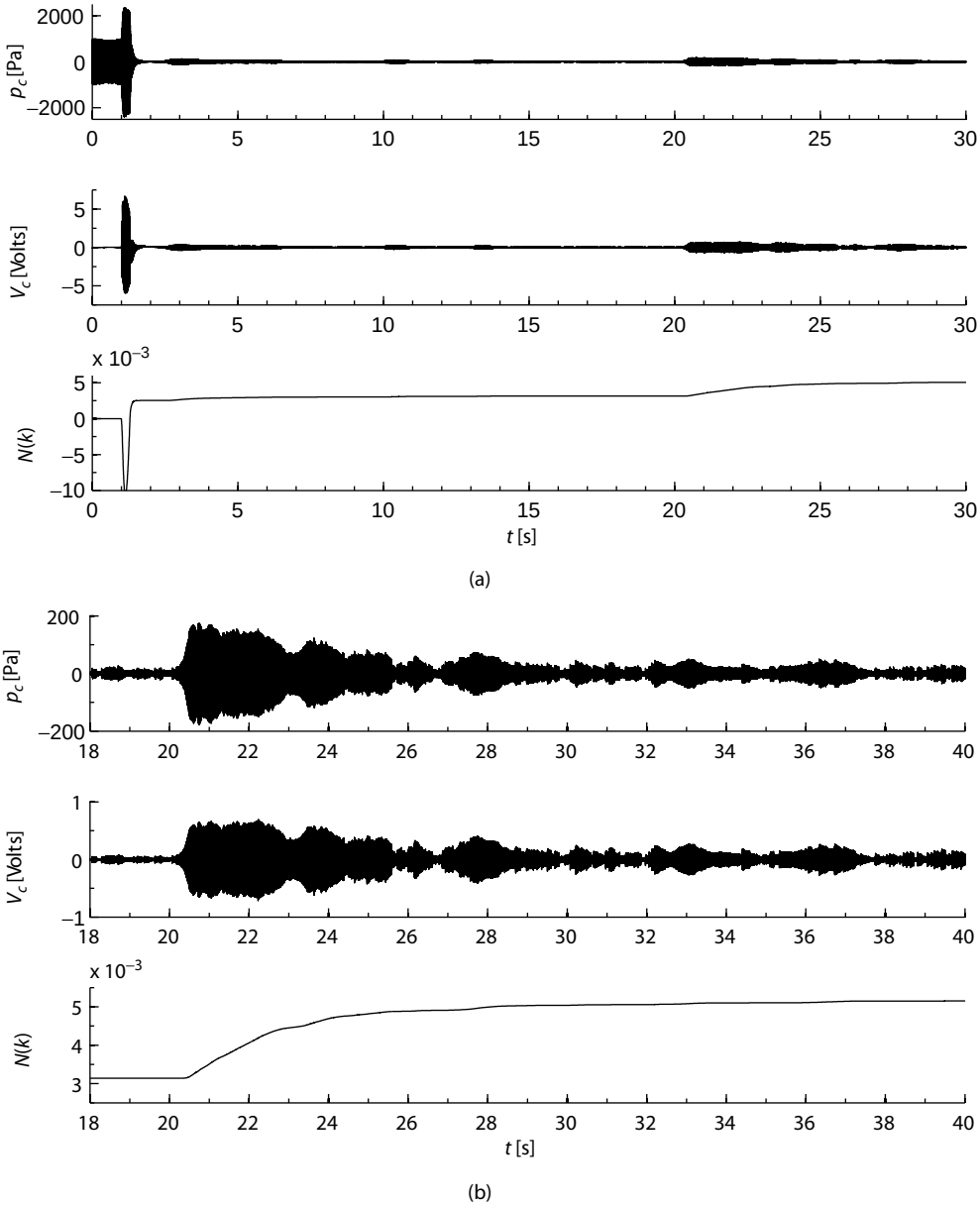

Figure 8: Experimental results for varying tube length ($N(k)$ initially updated in the wrong direction): (a) tube length increased at approximately 18s; and (b) zoomed-in plot of the controller's re-adaptation following the change in length. Legend same as figure 7.

within the limit cycle. The Nussbaum controller finds a stabilizing gain within approximately 0.4s. After approximately 18s, the length of the Rijke tube is increased. The Nussbaum gain is no longer stabilizing for this new length, but the controller re-adapts and finds a new stabilizing gain. This is seen more clearly in figure 8(b), which shows a zoomed-in section of figure 8(a). Here the time axis starts just before the length of the Rijke tube is increased.

5. CONCLUDING REMARKS

This paper has focused on feedback stabilization of thermoacoustic instability in a Rijke tube, and has done so using two quite different control approaches.

The first control approach is model-based, the focus being on finding low-order models that are useful for feedback control design. By using the Eigensystem Realization Algorithm (ERA) to find a *balanced* low-order model, a state-space model with just eight degrees of freedom is sufficient to capture the important input-output dynamics for feedback control design purposes.

The second approach employs adaptive control, which does not require a model, but instead requires that the system meet some general properties. Lyapunov-based adaptive control requires that the sign of the high frequency gain of the system is known: the focus here was on implementing an adaptive controller that did not require this information, and this was achieved using a Nussbaum gain.

It is encouraging that the model-based controller brings with it a similar level of robustness to changes in operating conditions as the adaptive controller, even though no adaptation of the controller takes place. The approach is also well-suited to real engine environments, where multiple sensors and multiple actuators may be required, since the state-space model (eqn (7)) admits multiple inputs and multiple outputs easily. A model of the system is required, however, and acquiring this can be challenging, particularly for an unstable system. The adaptive controller requires no such model, which is clearly an advantage. It does require that the system meet certain requirements, however, and these in themselves can be restrictive. The Nussbaum gain considered goes some way to reduce what must be known about the system, but makes the controller more complex, and may give rise to unnecessarily large control gains, which is to be avoided. (Although Appendix C goes some way to alleviate this.)

The order in which the two control strategies were presented may suggest that, in the authors' opinion, the adaptive controller represents a progression from the model-based controller. This is not the case. What is clear is that both strategies bring with them their own advantages and inconveniences, and one must consider carefully the physical system at hand when choosing a feedback control strategy.

ACKNOWLEDGEMENT

S.J. Illingworth gratefully acknowledges financial support from the Engineering and Physical Sciences Research Council (EPSRC) and Rolls-Royce plc. A.S. Morgans gratefully acknowledges the Royal Academy of Engineering and the EPSRC, who supported her as a Research Fellow throughout this work.

APPENDIX A. THE EIGENSYSTEM REALIZATION ALGORITHM

This section describes how the Eigensystem Realization Algorithm can be used to form balanced reduced-order models from input-output data of high-dimensional systems.

The starting point for the ERA is the generalized $\alpha q \times \beta p$ Hankel matrix composed of the system Markov parameters:

$$H(k-1) = \begin{bmatrix} Y_k & Y_{k+1} & \cdots & Y_{k+\beta-1} \\ Y_{k+1} & Y_{k+2} & \cdots & Y_{k+\beta} \\ \vdots & \vdots & \ddots & \vdots \\ Y_{k+\alpha-1} & Y_{k+\alpha} & \cdots & Y_{k+\alpha+\beta-2} \end{bmatrix} \tag{A.1}$$

where α and β are integers satisfying $\beta p \geq n$ and $\alpha q \geq n$, which ensures that $H(k-1)$ is of rank n. Recall that p is the number of inputs, q is the number of outputs, and n is the system order. The Markov parameter $Y_k \in \mathbb{R}^{q \times p}$ for time index k is defined as

$$Y_k \triangleq CA^{k-1}B. \tag{A.2}$$

See Juang [39] or Illingworth et al. [46] for how these Markov parameters can be found from input-output data. Setting $k = 1$ for the Hankel matrix, substituting in eqn (A.2) for the Markov parameters, and decomposing into two matrices, we find that

$$H(0) = \begin{bmatrix} C \\ CA \\ \vdots \\ CA^{\alpha-1} \end{bmatrix} \begin{bmatrix} B & AB & \cdots & A^{\beta-1}B \end{bmatrix} = \mathcal{P}_\alpha \mathcal{Q}_\beta, \tag{A.3}$$

where $\mathcal{P}_\alpha \in \mathbb{R}^{\alpha q \times r}$ is called the observability matrix and $\mathcal{Q}_\beta \in \mathbb{R}^{r \times \beta p}$ is called the controllability matrix of the high-order system of order r. The concepts of observability and controllability are

important for forming reduced-order models. The observability matrix $\mathcal{P}_\alpha$ is linked to the *measurement* of the state: a system is said to be observable if it is possible to recover its state from measurements of its inputs and outputs. The controllability matrix $\mathcal{Q}_\beta$ is linked to the *manipulation* of the state: a system is said to be controllable if any state x can be reached in a finite time when a suitable input is used.

Since the Hankel matrix $H(0)$ is composed of the Markov parameters in eqn (A.1), we see from eqn (A.3) that the Markov parameters are closely related to these observability and controllability matrices. For more details on the notions of observability and controllability, see Juang [39].

We now look at using the Eigensystem Realization Algorithm to form a reduced-order model of order $n < r$. The observability and controllability matrices of the reduced-order model will satisfy $\mathcal{P}_\alpha^T\mathcal{P}_\alpha = \mathcal{Q}_\beta\mathcal{Q}_\beta^T$. The reduced-order model is then called *balanced,* and this means that the input-output dynamics of the system that are important for feedback control are properly accounted for.

Factorizing the Hankel matrix $H(0)$, which has rank r, using the singular value decomposition, and truncating to order $n < r$, we have

$$H(0) = R\Sigma S^T \cong R_n\Sigma_n S_n^T. \tag{A.4}$$

R_n and S_n are made up of the first n (orthonormal) columns of R and S respectively. Σ_n is a rectangular matrix, $\Sigma_n = \text{diag} = [\sigma_1\ \sigma_2 \cdots \sigma_n]$, with $\sigma_1 \geq \sigma_2 \geq \cdots \geq \sigma_n > 0$, the first n singular values of $H(0)$. Examining equations (A.3) and (A.4) as a whole, we can write

$$H(0) = \mathcal{P}_\alpha\mathcal{Q}_\beta \cong (R_n\Sigma_n^{1/2})(\Sigma_n^{1/2}S_n^T). \tag{A.5}$$

One possible choice for the decomposition of $H(0)$ is then $\mathcal{P}_\alpha = R_n\Sigma_n^{1/2}$ and $\mathcal{Q}_\beta = \Sigma_n^{1/2}\,S_n^T$, and this choice makes both $\mathcal{P}_\alpha$ and $\mathcal{Q}_\beta$ balanced in the sense that

$$\begin{aligned}\mathcal{P}_\alpha^T\mathcal{P}_\alpha &= \Sigma_n^{1/2}R_n^TR_n\Sigma_n^{1/2} = \Sigma_n\\ \mathcal{Q}_\beta\mathcal{Q}_\beta^T &= \Sigma_n^{1/2}S_n^TS_n\Sigma_n^{1/2} = \Sigma_n.\end{aligned} \tag{A6}$$

$\mathcal{P}_\alpha^T\mathcal{P}_\alpha$ and $\mathcal{Q}_\beta\mathcal{Q}_\beta^T$ are called the observability and controllability Gramians of the reduced-order model, and are equal and diagonal by eqn (A.6)

The system matrices B and C can then be found from $\mathcal{Q}_\beta$ and $\mathcal{P}_\alpha$ in eqn (A.3). To find the A matrix, let $k = 2$ in eqn (A.1) and use eqn (A.5) to give

$$H(1) = \mathcal{P}_nA\mathcal{Q}_n \cong (R_n\Sigma_n^{1/2})A(\Sigma_n^{1/2}S_n^T),$$

from which A can be found. For a more rigorous treatment of the ERA, see Juang and Pappa [38] or Juang [39].

The state-space model (7) given by the ERA is *balanced*: the controllability and observability Gramians are diagonal and equal by eqn (A.6), and this means that the *dynamics* of the system are properly taken into account. Furthermore, an upper bound for the error in the reduced-order model can be derived. Let P_n denote the transfer function of the reduced-order model of order n, and let P_r denote the transfer function of the full system of order r. Then the $\mathcal{H}_\infty$-norm of the error satisfies

$$\left\|P_r - P_n\right\|_\infty \leq 2\sum_{j=n+1}^{r}\sigma_j,$$

('twice the sum of the tails'), where σ_j are the Hankel singular values of P_r.

APPENDIX B. PROOF OF CLOSED-LOOP STABILITY USING A NUSSBAUM GAIN

We consider the first order system (11). For the more general case of minimum phase, $n^* = 1$ systems, see [55]. The first order system (11) can be written in the time domain as

$$\dot{y}(t) = ay(t) + g_0u(t). \tag{B.1}$$

Suppose the adaptive control law

$$\dot{k}(t) = y^2(t)$$
$$u(t) = N(k)y(t)$$

is used, where $N(k)$ is a *Nussbaum gain*.[6] The resulting closed-loop system is given by

$$\dot{y}(t) = ay(t) + g_0 N(k)y(t) \tag{B.2}$$
$$\dot{k}(t) = y^2(t). \tag{B.3}$$

We want to find a Nussbaum gain that will guarantee closed-loop stability without knowledge of $\mathrm{sgn}(g_0)$. To study the closed-loop stability of the system, we introduce an indicator function,

$$\Lambda(t) = \frac{1}{2} y^2(t). \tag{B.4}$$

Evaluating $\dot{\Lambda}(t)$ along solutions to (B.2) gives

$$\begin{aligned}\dot{\Lambda}(t) &= y(t)\dot{y}(t) \\ &= \left\{a + g_0 N(k)\right\} y^2(t) \\ &= \left\{a + g_0 N(k)\right\} \dot{k}(t).\end{aligned}$$

Integrating over time t (using $k(0) = k_0$ and introducing $\sigma = k(\tau)$), we have

$$\int_0^t \dot{\Lambda}(\tau)d\tau = a\int_0^t \dot{k}(\tau)d\tau + g_0\int_0^t N(\sigma)\dot{k}(\tau)d\tau \tag{B.5}$$

$$= a[k(t) - k_0] + g_0\int_{k_0}^{k(t)} N(\sigma)d\sigma \tag{B.6}$$

and so

$$\Lambda(t) - \Lambda(0) = \left[k(t) - k_0\right]\left\{a + \frac{g_0}{k(t) - k_0}\int_{k_0}^{k(t)} N(\sigma)d\sigma\right\}. \tag{B.7}$$

Suppose that the Nussbaum gain $\mathrm{N}(\sigma)$ satisfies the two conditions

$$\begin{aligned}\sup_{k>k_0} \frac{1}{k - k_0}\int_{k_0}^{k} N(\sigma)d\sigma = \infty \\ \inf_{k>k_0} \frac{1}{k - k_0}\int_{k_0}^{k} N(\sigma)d\sigma = -\infty .\end{aligned} \tag{B8}$$

Seeking a contradiction, suppose that $k(t) \to \infty$ as $t \to \infty$ (from (B.3), $k(t)$ is monotone non-decreasing). Since the Nussbaum gain (B.8) takes arbitrarily large positive and negative values as $k(t) \to \infty$, we derive a contradiction at (B.7). Therefore $k(t)$ must be bounded. From (B.3), this is equivalent to $y(t) \in \mathcal{L}_2[0, \infty)$. Then from (B.2) $\dot{y}(t) \in \mathcal{L}_2[0, \infty)$. Finally, lemma 2.12 of Narendra and Annaswamy [51] shows that $y(t)$ is guaranteed to converge asymptotically to zero.

A similar proof can be used for the Lyapunov-based adaptive controller (eqn (12)) by replacing $N(k)$ by $-k(t)$ in eqn (B.2), setting $\dot{k}(\mathrm{t}) = \mathrm{sgn}(g_0)y^2(t)$ in eqn (B.3), and following the same procedure. (Although this is a departure from the standard proof, which employs a Lyapunov function, as discussed in §4.) The crucial difference is that this proof requires sgn (g_0).

[6] Note the positive feedback convention used here, which is the opposite of that used in eqn (12b). The Nussbaum gain is ultimately insensitive to the sign adopted, and we adopt a positive convention for simplicity.

APPENDIX C. ADAPTATION RATES FOR THE NUSSBAUM GAIN

The adaptation rates γ and μ, introduced into the adaptive controller's updating rule (14a) and control law (14b–14c) in §4.2 are now explained in more detail, together with details of how they are chosen.

Choosing γ

Looking at the updating rule (14a), one can see that γ sets the rate at which k adapts. Therefore γ can be set by specifying the desired speed of adaptation of k [58]. If k starts at zero, this corresponds to $3\tau_n$ for a 5% band around the set point (where τ_n is the period of the unstable mode):

$$\dot{k}(t) = \gamma\, p_c^2(t) = \frac{|k^*|}{3\tau_n}$$

and therefore

$$\gamma = \frac{|k^*|}{3\tau_n \hat{p}_c^2},$$

where k^* is the value of k for which closed-loop stability is achieved, and $\hat{p}_c$ is a characteristic value of p_c. The value of k^* will depend on whether the Nussbaum gain is initially updated in the right direction. To get around this we assume that the Nussbaum gain is initially updated in the right direction – then k^* will be similar in size to N^*, i.e.

$$\gamma = \frac{|N^*|}{3\tau_n \hat{p}_c^2}\ .$$

If the Nussbaum gain is initially updated in the wrong direction instead, then this simply means that the controller will take longer to reach k^* (and therefore N^*) and achieve closed-loop stability.

Choosing μ

Looking at the Nussbaum gain (14c), one can see that μ dictates, via the cosine term, exactly when $N(k)$ will switch sign. The Nussbaum gain $N(k)$ provides closed-loop stability by providing a gain that is (i) large enough and (ii) of the right sign. Furthermore, $N(k)$ only needs to switch sign once (if at all). Therefore it suffices to ensure, via μ, that $N(k)$ sweeps over a sufficiently large gain *before* it switches sign. This will allow the controller to 'try' a big enough gain before $N(k)$ switches sign.

We can ensure that this happens by specifying the turning point of $N(k)$, that is by specifying the value of $N(k)$ at which $\frac{dN}{dt} = 0$:

$$\frac{dN}{dt} = \frac{dN}{dk}\frac{dk}{dt} = 0.$$

We already have an expression for $\frac{dN}{dt}$ (14*a*) this is zero when p_c is zero. Therefore we are interested in $\frac{dN}{dk} = 0$. From (14c),

$$\frac{dN}{dk} = \cos(\mu|k_t|^{\frac{1}{4}}) - \frac{1}{4}\mu|k_t|^{\frac{1}{4}}\sin(\mu|k_t|^{\frac{1}{4}}) = 0\,,$$

where k_t is the k for which $\frac{dN}{dk} = 0$. Letting $\mu|k_t|^{\frac{1}{4}} = X$, we have

$$X\tan X = 4,$$

which we can solve for X. We need two equations for the two unknowns μ and k_t: the second equation comes from specifying N_t, the value of $N(k)$ for which $\frac{dN}{dk} = 0$, i.e.

$$N_t = N(k)\big|_{\frac{dN}{dk}=0} = k_t\cos(\mu|k_t|^{\frac{1}{4}})$$

$$N_t = k_t \cos X.$$

Then k_t and μ can be found using

$$k_t = \frac{N_t}{\cos X}$$

$$\mu = X\left|k_t\right|^{-\frac{1}{4}}.$$

Therefore to choose the two adaption rates γ and μ, it suffices to have an estimate (to order of magnitude accuracy only) of N^*, τ_n and $\hat{p}_c$. In addition, N_t needs to be chosen so that $N_t > |N^*|$ is guaranteed.

REFERENCES

1. Dowling, A.P., Ffowcs Williams, J.E.. *Sound and Sources of Sound*. Ellis Horwood; 1983.
2. Rayleigh, J.W.S.. *The Theory of Sound*. Macmillan and Co.; 1945.
3. Candel, S.M.. Combustion instabilities coupled by pressure waves and their active control. *Proc. Combust. Inst.* 1992;**24**(1):1277–1296.
4. Crocco, L.. Theoretical studies on liquid-propellant rocket instability. *Proc. Combust. Inst.* 1965;**10**:1101-1128.
5. Correa, S.M.. Power generation and aeropropulsion gas turbines: from combustion science to combustion technology. *Proc. Combust. Inst.* 1998;**27**:1793–1807.
6. Richards, G.A., Janus, M.C.. Characterization of oscillations during premix gas turbine combustion. *J. Eng. Gas Turbines Power* 1998;**120**(2):294–302.
7. Lieuwen, T., Neumeier, Y., Zinn, B.T.. The role of unmixedness and chemical kinetics in driving combustion instabilities in lean premixed combustors. *Combust. Sci. Technol.* 1998;**135**:193–211.
8. Broda, J.C., Seo, S., Santoro, R.J., Shirhattikar, G., Yang, V.. An experimental study of combustion dynamics of a premixed swirl injector. *Proc. Combust. Inst.* 1998;**27**:1849-1856.
9. McManus, K.R., Poinsot, T., Candel, S.M.. A review of active control of combustion instabilities. *Prog. Energy Combust. Sci.* 1993;**19**(1):1–29.
10. Dowling, A.P., Morgans, A.S.. Feedback control of combustion oscillations. *Annu. Rev. Fluid Mech.* 2005;**37**:151–182.
11. Dines, P.J.. *Active control of flame noise*. Ph.D. thesis; University of Cambridge; 1983.
12. Bloxsidge, G.J., Dowling, A.P., Hooper, N., Langhorne, P.J.. Active control of reheat buzz. *AIAA J.* 1988;**26**(7):783–790.
13. Poinsot, T., Bourienne, F., Candel, S., Esposito, E., Lang, W.. Suppression of combustion instabilities by active control. *J. Prop. Power* 1989; **5**(1):14-20.
14. Gulati, A., Mani, R.. Active control of unsteady combustion-induced oscillations. *J. Prop. Power* 1992;**8**:1109–1115.
15. Annaswamy, A.M., Fleifil, M., Rumsey, J.W., Prasanth, R., Hathout, J., Ghoniem, A.F.. Thermoacoustic instability: model-based optimal control designs and experimental validation. *IEEE Trans. Contr. Syst. Technol.* 2000;**8**(6):905–918.
16. Morgans, A.S., Dowling, A.P.. Model-based control of combustion instabilities. *J. Sound Vib.* 2007;**299**:261–282.
17. Chu, Y.C., Glover, K., Dowling, A.P.. Control of combustion oscillations via $\mathcal{H}_\infty$ loop-shaping, μ-analysis and integral quadratic constraints. *Automatica* 2003;**39**(2):219–231.
18. Campos-Delgado, D.U., Zhou, K., Allgood, D., Acharya, S.. Active control of combustion instabilities using model-based controllers. *Combust. Sci. Technol.* 2003;**175**(1):27–53.
19. Murugappan, S., Acharya, S., Allgood, D.C., Park, S., Annaswamy, A.M., Ghoniem, A.F.. Optimal control of a swirl-stabilized spray com-bustor using system identification approach. *Combust. Sci. Technol.* 2003;**175**(1):55–81.

20. Hathout, J.P., Annaswamy, A.M., Fleifil, M., Ghoniem, A.F.. A model-based active control design for thermoacoustic instability. *Combust. Sci. Technol.* 1998;**132**:99–138.
21. Tierno, J.E., Doyle, J.C.. Multi mode active stabilization of a Rijke tube. *Active Control of Noise and Vibration, 1992: presented at the ASME Winter Annual Meet* 1992;**38**:65–68.
22. Billoud, G., Galland, M.A., Huu, C.H., Candel, S.. Adaptive active control of combustion instabilities. *Combust. Sci. Technol.* 1992;**81**(4):257–283.
23. Liu, G.P., Daley, S.. Output-model-based predictive control of unstable combustion systems using neural networks. *Contr. Eng. Pract.* 1999;**7**(5):591–600.
24. Neumeier, Y., Zinn, B.T.. Experimental demonstration of active control of combustion instabilities using real-time modes observation and secondary fuel injection. *Proc. Combust. Inst.* 1996;**26**:2811–2818.
25. Krstic, M., Krupadanam, A., Jacobson, C.. Self-tuning control of a nonlinear model of combustion instabilities. *IEEE Trans. Contr. Syst. Technol.* 1999;**7**(4):424–436.
26. Annaswamy, A.M., El Rifai, O.M., Fleifil, M., Hathout, J.P., Ghoniem, A.F.. A model-based self-tuning controller for thermoacoustic instability. *Combust. Sci. Technol.* 1998;**135**:213–240.
27. Evesque, S., Dowling, A.P., Annaswamy, A.M.. Self-tuning regulators for combustion oscillations. *Proc. R. Soc. A* 2003;**459**(2035):1709–1749.
28. Howe, M.S.. *Acoustics of Fluid-Structure Interactions*. Cambridge University Press; 1998.
29. Heckl, M.A.. Active control of the noise from a Rijke tube. *J. Sound Vib.* 1988;**124**:117–33.
30. Dowling, A.P.. Nonlinear self-excited oscillations of a ducted flame. *J. Fluid Mech.* 1997;**346**: 271–290.
31. Skogestad, S., Postlethwaite, I.. *Multivariable Feedback Control: Analysis and Design*. Wiley; 2005.
32. Morgans, A.S., Annaswamy, A.M.. Adaptive control of combustion instabilities for combustion systems with right-half plane zeros. *Combust. Sci. Technol.* 2008;**180**(9):1549–1571.
33. Langhorne, P.J., Dowling, A.P., Hooper, N.. A practical active control system for combustion oscillations. *J. Prop. Power* 1990;**6**(3):324–333.
34. Van Den Hof, P.M.J., Schrama, R.J.P.. Identification and control–closed-loop issues. *Automatica* 1995;**31**(12):1751–1770.
35. Vinnicombe, G.. *Uncertainty and Feedback: $\mathcal{H}_\infty$ loop-shaping and the ν-gap metric*. Imperial College Press; 2000.
36. Rowley, C.W.. Model reduction for fluids, using balanced proper orthogonal decomposition. *Int. J. Bifurc. Chaos* 2005;**15**(3):997–1013.
37. Ma, Z., Ahuja, S., Rowley, C.W.. Reduced order models for control of fluids using the Eigensystem Realization Algorithm. *Theor. Comp. Fluid Mech.* 2009;.
38. Juang, J.N., Pappa, R.S.. Eigensystem Realization Algorithm for modal parameter identification and model reduction. *J. Guid. Contr. Dyn.* 1985;**8**(5):620–627.
39. Juang, J.N.. *Applied System Identification*. Prentice Hall; 1994.
40. Cattafesta III, L.N., Garg, S., Choudhari, M., Li, F.. Active control of flow-induced cavity resonance. *AIAA paper 97-1804* 1997;.
41. Cabell, R.H., Kegerise, M.A., Cox, D.E., Gibbs, G.P.. Experimental feedback control of flow-induced cavity tones. *AIAA J.* 2006;**44**(8):1807–1815.
42. Gaitonde, A.L., Jones, D.P.. Reduced order state-space models from the pulse responses of a linearized CFD scheme. *Internat. J. Numer. Methods Fluids* 2003;**42**(6):581–606.
43. Silva, W.A., Bartels, R.E.. Development of reduced-order models for aeroelastic analysis and flutter prediction using the CFL3Dv6.0 code. *J. Fluids Struct.* 2004;**19**(6):729–745.
44. Ma, Z.. *Reduction and reconstruction methods for simulation and control of fluids*. Ph.D. thesis; Princeton University; 2010.
45. Illingworth, S.J.. *Feedback control of oscillations in combustion and cavity flows*. Ph.D. thesis; University of Cambridge; 2010.

46. Illingworth, S.J., Morgans, A.S., Rowley, C.W.. Feedback control of flow resonances using balanced reduced-order models. *J. Sound Vib*. 2011;**330**:1567–1581.
47. Ljung, L.. *System Identification: Theory for the User, Second Ed*. Prentice-Hall; second ed.; 1999.
48. Doyle, J.. Guaranteed margins for LQG regulators. *IEEE Trans. Automat. Contr.* 1978;**23**(4): 756–757.
49. Riley, A.J., Park, S., Dowling, A.P., Evesque, S., Annaswamy, A.M.. Advanced closed-loop control on an atmospheric gaseous lean-premixed combustor. *J. Eng. Gas Turbines Power* 2004;**126**:708–716.
50. Illingworth, S.J., Morgans, A.S.. Adaptive feedback control of combustion instability in annular combustors. *Combust. Sci. Technol*. 2010;**182**(2):143–164.
51. Narendra, K.S., Annaswamy, A.M.. *Stable Adaptive Systems*. Dover Publications; 1989.
52. Dorf, R.C., Bishop, R.H.. *Modern Control Systems*. Pearson Prentice Hall; 2005.
53. Morse, A.S.. Recent problems in parameter adaptive control. *Outils et Modèles Mathématiques pour l'Automatique, l'Analyse de Systèmes et le Traitement du Signal* 1983;**3**:733–740.
54. Nussbaum, R.D.. Some remarks on a conjecture in parameter adaptive control. *Syst. Contr. Letters* 1983;**3**(5):243–246.
55. Willems, J.C., Byrnes, C.I.. Global adaptive stabilization in the absence of information on the sign of the high frequency gain. *Lect. Notes Control. Inform. Sci*. 1984;62:49-57.
56. Ilchmann, A.. *Wiley Encyclopedia of Electrical and Electronics Engineering;* vol. 21; chap. Switching Functions. Wiley; 1999, p. 213–219.
57. Ioannou, P., Sun, J.. *Robust Adaptive Control*. Prentice Hall; 1996.
58. Yildiz, Y., Annaswamy, A.M., Yanakiev, D., Kolmanovsky, I.. Adaptive idle speed control for internal combustion engines. *Am. Contr. Confer.* 2007;:3700–3705.